Nanotube field and orientational properties of C_{70} molecules in carbon nanotubes

B. Verberck and K. H. Michel
Department of Physics, University of Antwerp, Groenenborgerlaan 171, 2020 Antwerpen, Belgium
(Received 12 September 2006; published 16 January 2007)

The orientation of a C_{70} fullerene molecule encapsulated in a single-walled carbon nanotube (SWCNT) depends on the tube radius. First we confirm that chirality effects do not affect the orientation as well by comparing discrete atomistic calculations with the results of a continuous tube approximation for a variety of SWCNTs. The molecular and the tube symmetry are exploited by using symmetry-adapted rotator functions. We accurately determine the optimal molecular orientation as a function of the tube radius; for low ($\lesssim$7 Å) and high ($\gtrsim$7.2 Å) tube radii, lying and standing molecular orientations are recovered, respectively. In between, we observe a transition regime. In addition, we consider off-axis positions. We perform a one-dimensional liquid description of a chain of on-axis C_{70} molecules inside a SWCNT. All results agree well with recent x-ray diffraction experiments.

DOI: 10.1103/PhysRevB.75.045419 PACS number(s): 61.48.+c

I. INTRODUCTION

The followup of Iijima's 1991 discovery of carbon nanotubes (CNTs)[1] has been their filling with atoms and/or molecules. The resulting hybrid materials often exhibit one-dimensional (1D) characteristics and are at present the subject of fundamental studies as well as more application-oriented research. For a review on CNTs and their filling and on earlier work on carbon fibers[2] we refer to Refs. 3–6. The insertion of fullerene molecules into CNTs, and specifically into single-walled carbon nanotubes (SWCNTs), is of particular interest since the resulting structures—the so-called "peapods"[7]—consist of carbon only. C_{60} peapods $[(C_{60})_N$@SWCNT] were observed first[7] and have received most of the attention. Nevertheless, other fullerene molecules have been succesfully inserted into SWCNTs as well, e.g., C_{70},[8,9] C_{76}, C_{78}, C_{80}, C_{82}, and C_{84}.[9]

In this paper we focus on C_{70} peapods. While a C_{60} molecule can be considered as spherical, a C_{70} molecule—differing from C_{60} by the presence of an extra "belt" of 10 C atoms, Fig. 1—resembles an ellipsoid. Indeed, one can distinguish a long and a short axis. The C_{70} molecule's aspherical shape is expected to strongly dictate its orientation inside a SWCNT: for small tube radii, short-range repulsive forces make the molecule's long axis lie parallel to the tube's long axis, while for larger radii, long-range attractive van der Waals forces flip the molecule to an orientation where the molecule's long axis is perpendicular to the tube's long axis. While these respective "lying" and "standing" orientations (Fig. 2) have been experimentally observed from the start[9,10] and later on,[11–14] a quantitative answer to the question at which radius R_T exactly the molecular orientation changes from lying to standing has been given only very recently by x-ray diffraction experiments and related theoretical work.[15,16] Also, the possibility of having intermediate orientations [Fig. 2(b)] was only considered in Ref. 15.

Theoretically reproducing the orientations of a C_{70} molecule requires calculating its potential energy due to the interaction with the surrounding CNT—the molecule's "nanotube field." In Refs. 17 and 18, an approximative calculation of the nanotube field of a rigid C_{60} molecule inside a SWCNT was presented: the tube was treated as a homogeneous cylindrical carbonic surface density while the structural (icosahedrally symmetric) features of the C_{60} molecule were retained. In Ref. 19 we verified the validity of this "smooth-tube approach" and concluded it to work well for intermediate and large tube radii ($R_T \gtrsim 7$ Å) and still acceptably for small tubes. The smooth-tube approximation can be applied to C_{70}@SWCNT as well. Intuitively, it might even work better than for C_{60}@SWCNT since the changes in molecular orientation, adequately accounted for by the discrete molecular structure, are expected to dominate the tube-molecule interaction energy more because of the ellipsoidal rather than the spherical molecular shape.

In this work we apply the smooth-tube approximation to C_{70}@SWCNT and compare it with calculations taking the true CNT structure into account (Secs. II–IV). We discuss lowest-energy orientations of a single molecule and examine

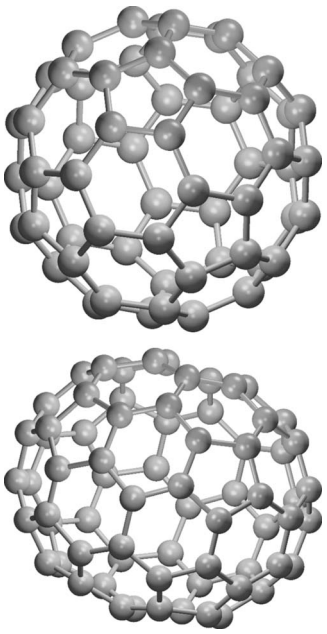

FIG. 1. While a C_{60} molecule (top) is highly spherical, a C_{70} molecule (bottom) has an ellipsoidal shape.

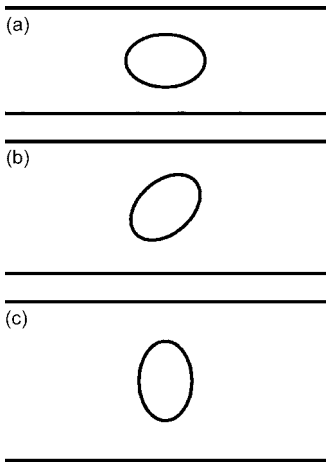

FIG. 2. Orientations of a C_{70} molecule (represented as an ellipse) inside a SWCNT (horizontal lines): (a) lying, (b) intermediate, (c) standing.

molecular positions off the tube's long axis (Sec. V). Comparisons with the recent experimental and theoretical results, in particular with those of Chorro *et al.*,[15] are made. In Sec. VI we investigate the consequences of the nanotube field on multimolecule systems, i.e., $(C_{70})_N$@SWCNT peapods. Finally, we present general conclusions (Sec. VII).

II. NANOTUBE FIELD: ATOMISTIC FORMULATION

We consider a single C_{70} molecule encapsulated in a SWCNT; the molecule's center of mass lies on the tube's long axis. Our goal is to investigate how the molecular potential energy due to its interaction with the tube wall changes when the molecule adopts various orientations.

Any molecular orientation is characterized by three Euler angles, α, β and γ. We use the convention of Ref. 20: the three Euler rotations are (i) a rotation over $0 \leqslant \alpha < 2\pi$ about the z axis, followed by (ii) a rotation over $0 \leqslant \beta \leqslant \pi$ about the y axis, and finally (iii) a rotation over $0 \leqslant \gamma < 2\pi$ about the z axis again. The x, y, and z axes are kept fixed. The z axis of a Cartesian (x,y,z) axis system is chosen to coincide with the tube's long axis. As the starting orientation, $\alpha=\beta=\gamma=0$, we take the orientation depicted in Fig. 3—called "standard orientation:" the C_{70} molecule's fivefold axis coincides with the tube's long axis and the "pentagons" perpendicular to the z axis each have one atom with coordinates $(x>0,\ y=0)$. In this paper we use the atomic coordinates of Ref. 21, obtained from powder neutron diffraction data on C_{70} fullerite.

A SWCNT with chiral indices (n,m) can be obtained by rolling up a graphene sheet with basis vectors $\mathbf{a}_1=a\mathbf{e}_X$ and $\mathbf{a}_2=a\frac{1}{2}\mathbf{e}_X+a\frac{3}{2}\mathbf{e}_Y$, where $\mathbf{e}_X$ and $\mathbf{e}_Y$ are planar cartesian basis vectors, along the vector $\mathbf{C}(n,m)=n\mathbf{a}_1+m\mathbf{a}_2$.[3,22] The distance $a=2.49$ Å is related to the C–C bond length d_{CC} in graphene: $d_{CC}=a/\sqrt{3}=1.44$ Å.[3,22]. We position the resulting tube so that the C atom originally (before rolling up) at $0\mathbf{e}_X+0\mathbf{e}_Y$ lies in the (x,y) plane with x coordinate 0 and y coordinate R_T—the tube's radius—and so that the cylinder containing the C atoms has its long axis coinciding with the z axis.

The foregoing settles the (x,y,z) coordinate system, the arrangement of the carbon nanotube, and the starting orientation of the C_{70} molecule. It also implicitly fixes the molecule's initial position along the tube axis. However, for an infinite nanotube, any position obtained by a shift, say ζ, along the z axis should be treated on the same footing as the original one $(\zeta=0)$. The interaction energy of the C_{70} molecule therefore generally depends on the four variables α, β, γ, and ζ, and on the tube indices n and m:

$$V_{\mathrm{NF}} \equiv V_{\mathrm{NF}}(\alpha,\beta,\gamma;\zeta;n,m). \tag{2.1}$$

The subscript NF stands for "nanotube field." Indeed, the interaction energy can be interpreted as an energy field set up by the nanotube surrounding the C_{70} molecule.

The interaction between the C_{70} molecule and the nanotube is of van der Waals-type [high-resolution transmission electroscopy (HRTEM) observations of peapods reveal the motion of the fullerene molecules along the tube axis and rule out chemical bonds[9]]. The most simple way to describe the interaction of the molecule with the nanotube and to take into account the discrete structure of the molecule, is to take the atoms of the molecule as point centers which interact with the atoms of the nanotube (we call these point centers on the molecule "atomic interaction centers"). Assuming atom-atom pair interactions, the total interaction energy reads

$$V_{\mathrm{NF}} = \sum_{\Lambda_a=1}^{70} \sum_{\tau} v^a(|\mathbf{r}_\tau - \mathbf{r}_{\Lambda_a}|), \tag{2.2}$$

where $\Lambda_a=1,\ \ldots,\ N_a,\ N_a=70$, indexes the 70 C atoms of the molecule and τ the C atoms of the tube. In Eq. (2.2), $\mathbf{r}_\tau$ and $\mathbf{r}_{\Lambda_a}$ are the position vectors of atom τ of the nanotube and atom Λ_a of the molecule, respectively. The van der Waals pair potential v^a only depends on the interatomic distance $|\mathbf{r}_\tau - \mathbf{r}_{\Lambda_a}|$. Following Ref. 23, we treat certain bonds of the C_{70} molecule as point interaction centers (ICs) too. They were originally introduced to account for charge-density variations on C–C bonds within a C_{70} molecule when studying C_{70}–C_{70} interactions in C_{70} fullerite (solid C_{70}) by means of molecular-dynamics simulations.[23] Each of the two C_{60}-like hemispheres ("caps") features 10 "D centers" (similar to "double-bond" ICs in C_{60}[24]), while the belt region is populated with 30 "I centers," see Fig. 4. We label the 20 D centers and the 30 I centers by the indices $\Lambda_D=1,\ \ldots,\ N_D$, $N_D=20$, and $\Lambda_I=1,\ \ldots,\ N_I,\ N_I=30$, respectively. Since the D and I centers are defined as midpoints of certain bonds (see Fig. 4), their coordinates can be simply calculated from the atomic coordinates. The generalization of Eq. (2.2) reads

$$V_{\mathrm{NF}} = \sum_{t=a,D,I} \sum_{\Lambda_t=1}^{N_t} \sum_{\tau} v^t(|\mathbf{r}_\tau - \mathbf{r}_{\Lambda_t}|), \tag{2.3}$$

with t indexing the type of IC of the C_{70} molecule. For the type-dependent pair interactions we use Born-Mayer-van der Waals potentials:

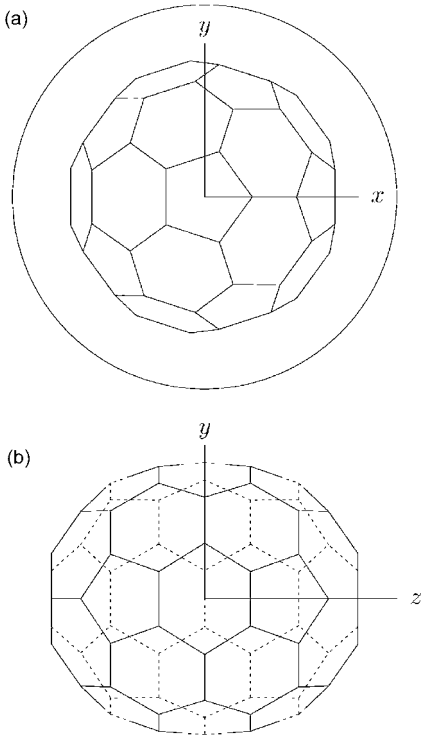

FIG. 3. A C_{70} molecule, in standard orientation, in a nanotube: (a) projection onto the (x,y) plane, (b) projection onto the (y,z) plane. The surrounding tube is drawn schematically as a circle (a) and horizontal lines (b). In (b), bonds lying above the (y,z) plane $(x<0)$ are shown dashed.

$$v^t(r) = C_1^t e^{-C_2^t r} - \frac{B^t}{r^6}. \tag{2.4}$$

The set of potential constants used here is a modification of the set used in Ref. 25 and is tabulated in Table I. Note that in the present description, the carbon nanotube does not exhibit bond ICs, i.e., the 70+20+30 ICs of the C_{70} molecule interact only with the tube's C atoms.

In Eq. (2.3), the sum over tube atoms—with coordinates $\mathbf{r}_\tau=(x_\tau,y_\tau,z_\tau)$—can be restricted to atoms in a certain vicinity of the C_{70} molecule, realized by imposing the criterion

$$z_{\min} \leqslant z_\tau \leqslant z_{\max}, \tag{2.5}$$

with $z_{\min}$ and $z_{\max}$ cutoff values ensuring convergence. We denote the resulting number of atoms then taken into account by N_T.

We have now gathered all ingredients for the calculation of V_{NF} for given α, β, γ, ζ, n, and m. Before discussing results obtained via this way, we present an alternative—approximative—formalism in the next section, involving symmetry-adapted rotator functions (SARFs).

III. NANOTUBE FIELD: CONTINUOUS FORMULATION

As seen in the previous section, the nanotube field V_{NF} generally depends on six variables. The number of variables can be halved by neglecting the nanotube's discrete structure. Indeed, if one assumes a continuous distribution of carbon

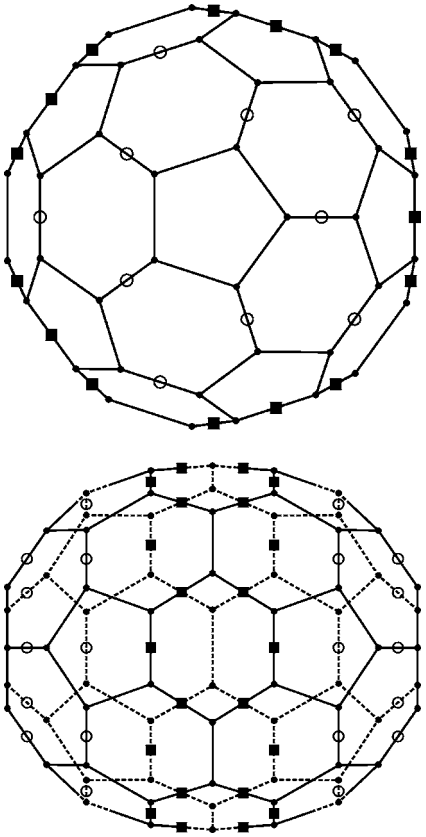

FIG. 4. Interaction centers of a C_{70} molecule. The same projections as in Fig. 3 are shown. Apart from the 70 atoms, 20 D centers (circles) and 30 I centers (squares) are considered.

atoms on a cylinder, the indices n and m are replaced by the radius R_T, and the translational coordinate ζ and one of the Euler angles become irrelevant. We distinguish this "smooth-tube" approach from the "discrete-tube" approach described in the preceding section by adding superscripts:

$$V_{\mathrm{NF}}^{\mathrm{smooth}} \equiv V_{\mathrm{NF}}(\beta,\gamma;R_T), \tag{3.1a}$$

$$V_{\mathrm{NF}}^{\mathrm{discrete}} \equiv V_{\mathrm{NF}}(\alpha,\beta,\gamma;\zeta;n,m). \tag{3.1b}$$

A continuum approximation for the nanotube in combination with a discrete structure of the fullerene was first introduced in Refs. 17 and 18 for the description of C_{60}@SWCNT peapods; its validity was tested in detail in Ref. 19. We point out that using the smooth-tube approach, where a tube is characterized by its radius R_T rather than its indices n and m, somehow reflects today's experimental situation: while the production of nanotubes (and peapods) with a distribution of

TABLE I. Potential constants C_1, C_2, and B, used for modelling C_{70}-SWCNT interactions.

t	a	D	I
C_1^t ($\times 10^6$ K)	9.65	6.24	0.84
C_2^t ($\mathrm{Å}^{-1}$)	3.6	3.4	3.5
B^t ($\times 10^5$ K $\mathrm{Å}^6$)	1.28	0	0

radii around a certain value can be realized, it is up to now still impossible to manufacture nanotubes (let alone peapods) with a given pair of chiral indices (n,m). It is only possible to determine the chiral indices of a grown nanotube a posteriori, say by Raman scattering—for a review, see Ref. 26. Here we give formulas for the smooth-tube approximation; the validity of the approach for C_{70}@SWCNT systems will be discussed in the next section.

The radius R_T of a tube with indices (n,m) reads

$$R_T = \frac{a}{2\pi}\sqrt{n^2+nm+m^2}. \tag{3.2}$$

The surface density σ—common for all carbon nanotubes, i.e., radius-independent—can be readily calculated to be

$$\sigma = \frac{4}{\sqrt{3}a^2} = 0.372\ \text{Å}^{-2}. \tag{3.3}$$

The nanotube field itself is then obtained by

$$V_{\mathrm{NF}}^{\mathrm{smooth}}(R_T) = \sigma R_T \sum_t \sum_{\Lambda_t} \int_0^{2\pi} d\Phi \int_{-\infty}^{+\infty} dZ v^t(|\boldsymbol{\rho} - \mathbf{r}_{\Lambda_t}|), \tag{3.4}$$

where $\boldsymbol{\rho}$ is the position vector of a point on the cylindrical tube ($\rho_x = R_T \cos\Phi$, $\rho_y = R_T \sin\Phi$, $\rho_z = Z$). Analogous to limiting the summation over tube atoms in Eq. (2.3) via criterion (2.5), the integral over Z in Eq. (3.4) can be limited to the interval $z_{\min} \leqslant Z \leqslant z_{\max}$. In the Appendix, we show that Eq. (3.4) can be elaborated into the following form:

$$V_{\mathrm{NF}}^{\mathrm{smooth}}(\beta,\gamma;R_T) = \sigma R_T \sum_t \sum_{\lambda_t} \sum_{l=0,2,4,}^{\infty} w_l^t(\lambda_t,R_T)\mathcal{U}_l^t(\lambda_t;\beta,\gamma). \tag{3.5}$$

Here, the index λ_t refers to "layers" of ICs of type t: layers are defined to contain all ICs with equal $|z_{\Lambda_t}|$ values (see the Appendix). The SARFs $\mathcal{U}_l^t(\lambda_t;\beta,\gamma)$ are linear combinations of spherical harmonics; they account for the symmetry of the molecule and of the nanotube:

$$\mathcal{U}_l^t(\lambda_t;\beta,\gamma) = \sqrt{\frac{4\pi}{2l+1}} \sum_{n=-l}^{l} \alpha_l^{t,n}(\lambda_t) Y_l^n(\beta,\gamma). \tag{3.6}$$

Inversion symmetry of the smooth nanotube implies that only even values of l occur. The D_{5h} symmetry of the C_{70} molecule imposes the following selection rule[27–29] on the multipole coefficients $\alpha_l^{t,n}(\lambda_t)$:

$$\alpha_l^{t,n}(\lambda_t) \neq 0 \quad \text{if } l+n \text{ even and } n = 0, \pm 5, \pm 10, \ldots . \tag{3.7}$$

Hence for the case of the peapod with the smooth tube approximation, $\alpha_l^{t,n}(\lambda_t) \neq 0$ for l even, and $n = 0, \pm 10, \ldots$. In Eq. (3.5) the pair potential parameters are contained within the coefficients $w_l^t(\lambda_t,R_T)$.[30] A serious advantage of the SARFs expansion, Eq. (3.5), is that a limited number of terms (say up to $l=10$) already give extremely good convergence. We point out that, apart from introducing physical-mathematical transparency, expansion (3.5) provides a much more efficient (less time-consuming) way of calculating $V_{\mathrm{NF}}^{\mathrm{smooth}}$ than by directly performing coordinate transforms and evaluating Eq. (3.4).

IV. ATOMISTIC VS CONTINUUM APPROACH: RESULTS

We have calculated the nanotube field of a centrally positioned C_{70} molecule inside a SWCNT, both via the atomistic and the continuum approach [Eqs. (2.3) and (3.5), respectively], for a representative selection of tubes with radii in the range $6.5\ \text{Å} \lesssim R_T \lesssim 11\ \text{Å}$. Relevant tube characteristics of our selected tubes are listed in Table II. As discussed in the previous sections, the smooth-tube approach has the advantage of resulting in a nanotube field depending only on (β,γ) and R_T. Hence, for a given tube radius, the nanotube field can be visualized as a (β,γ) Mercator map.[36] The discrete-tube approach on the other hand displays full (α,β,γ) and ζ dependence. To be able to make preliminary (visual) comparisons between the two approaches, we have first put $\alpha=0$ and $\zeta=0$. We have used the value $-z_{\min}=z_{\max}=50$ Å [see Eq. (2.5)]; they ensure sufficient convergence, the numbers of tube atoms N_T then are of the order of a few thousand. Figure 5 shows $V_{\mathrm{NF}}^{\mathrm{discrete}}(\alpha=0,\beta,\gamma;\zeta=0;n,m)$ and $V_{\mathrm{NF}}^{\mathrm{smooth}}(\beta,\gamma;R_T)$ for (14, 4), (19, 0), and (11, 11) tubes. Although small differences between the discrete and the smooth approaches are present, the overall agreement is very good; also, the energy ranges match. These observations hold for all pairs of $(V_{\mathrm{NF}}^{\mathrm{discrete}}, V_{\mathrm{NF}}^{\mathrm{smooth}})$ maps; overall agreement and matching of energy boundaries is seen for all investigated tubes. The worst matching occurs for the (18, 0) tube, the nanotube fields of which are shown in Fig. 6, but even then the smooth-tube approximation works well. The variations $\Delta_{\beta\gamma}$, defined as the difference between the maximum and the minimum values of $V_{\mathrm{NF}}^{\mathrm{discrete}}(\alpha=0,\beta,\gamma;\zeta=0;n,m)$ in the interval $(0 \leqslant \beta \leqslant \pi, 0 \leqslant \gamma \leqslant 2\pi)$, are tabulated in Table II.

A feature seen in all Mercator maps is the very weak dependence of V_{NF} on γ. Apparently, an initial molecular rotation about the z axis over $-\gamma$ has almost no influence on the nanotube field, while a subsequent rotation about the y axis over $-\beta$ has a high impact. Recalling that a C_{70} molecule can be thought of as an ellipsoidal object, we note that these Euler rotations are performed about the long and a short ellipsoidal axis, respectively, which intuitively explains the respective weak and strong effect of the γ and the β rotation. Mathematically, the weak $V_{\mathrm{NF}}(\gamma)$ dependence can be traced to the $\alpha_l^{t,n}$ coefficients [Eq. (3.7)]. Indeed, for $l<10$ no $\alpha_l^{t,n\neq 0}(\lambda_t)$ coefficient, and hence no γ dependence, is present in the SARFs expansion. Only from $l=10$ onwards, $n \neq 0$ coefficients enter the expansion: $(l=10,n=0)$, $(l=10,n=\pm 10)$, $(l=12,n=0)$, $(l=12,n=\pm 10)$, etc., yield nonvanishing $\alpha_l^{t,n}(\lambda_t)$ coefficients. This observation and the diminishing magnitude of the expansion coefficients w_l^t for increasing l explains the weak γ dependence.

The foregoing ignores any possible α and/or ζ dependence of V_{NF}. Intuitively, we expect these degrees of freedom to have a lesser importance since the $V_{\mathrm{NF}}^{\mathrm{discrete}}(\alpha=0,\beta,\gamma;\zeta=0)$ Mercator maps already display good agreement with

TABLE II. Characteristics of selected (n,m) tubes. Tubes of all types (zigzag, chiral, and armchair) with radii R_T as close to $6.5, 7.0, \ldots, 11.0$ Å as possible were chosen. The index i is introduced for convenience. Definitions of the the translational period T_T (units Å) and energy ranges $\Delta_{\beta\gamma}$ and $\Delta_{\alpha\zeta}$ (units K) are given in the text.

i	(n,m)	Chirality	R_T (Å)	T_T (Å)	$\Delta_{\beta\gamma}$ (K)	$\Delta_{\alpha\zeta}$ (K)
1	(14,4)	Chiral	6.4876	35.3018	46 189.502	2.076
2	(16,3)	Chiral	7.0112	76.3013	2652.450	0.101
3	(16,5)	Chiral	7.5296	81.9433	3082.674	2.836
4	(15,8)	Chiral	8.0146	87.2211	2685.575	0.164
5	(21,1)	Chiral	8.5273	92.8005	1779.479	0.103
6	(16,10)	Chiral	9.0021	16.3280	1171.780	0.035
7	(19,8)	Chiral	9.5194	103.5972	753.531	0.115
8	(17,12)	Chiral	10.0021	108.8503	511.659	0.120
9	(21,7)	Chiral	10.0021	15.5500	511.659	0.037
10	(23,4)	Chiral	10.0021	108.8503	511.659	0.120
11	(23,6)	Chiral	10.5074	114.3504	350.457	0.126
12	(26,1)	Chiral	10.5074	114.3504	350.457	0.126
13	(17,15)	Chiral	10.9896	119.5978	250.073	0.132
14	(17,0)	Zigzag	6.7370	$\sqrt{3}a=4.3128$	16 170.658	16.786
15	(18,0)	Zigzag	7.1333	$\sqrt{3}a$	511.129	2.611
16	(19,0)	Zigzag	7.5296	$\sqrt{3}a$	3086.232	0.352
17	(20,0)	Zigzag	7.9259	$\sqrt{3}a$	2841.527	0.036
18	(21,0)	Zigzag	8.3222	$\sqrt{3}a$	2120.746	0.008
19	(23,0)	Zigzag	9.1148	$\sqrt{3}a$	1062.206	0.006
20	(24,0)	Zigzag	9.5111	$\sqrt{3}a$	758.702	0.006
21	(25,0)	Zigzag	9.9074	$\sqrt{3}a$	550.902	0.006
22	(26,0)	Zigzag	10.3037	$\sqrt{3}a$	406.917	0.006
23	(28,0)	Zigzag	11.0963	$\sqrt{3}a$	232.745	0.006
24	(9,9)	Armchair	6.1776	$a=2.49$	143 905.001	49.357
25	(10,10)	Armchair	6.8640	a	8075.480	4.489
26	(11,11)	Armchair	7.5504	a	3104.614	0.017
27	(12,12)	Armchair	8.2369	a	2274.001	0.002
28	(13,13)	Armchair	8.9233	a	1255.697	0.002
29	(14,14)	Armchair	9.6097	a	699.526	0.002
30	(15,15)	Armchair	10.2961	a	409.231	0.002
31	(16,16)	Armchair	10.9825	a	251.288	0.002

their $V_{\mathrm{NF}}^{\mathrm{smooth}}(\beta,\gamma)$ counterparts. Nevertheless, a systematic inquiry is in order. For all tubes listed in Table II, we have calculated $V_{\mathrm{NF}}^{\mathrm{discrete}}(\alpha,\beta=0,\gamma=0;\zeta)$ for $0\leqslant\alpha\leqslant 2\pi$ and $0\leqslant\zeta\leqslant T_T$, where T_T is the nanotube's translational period. While T_T is small for nonchiral—i.e., zigzag, $T_T=\sqrt{3}a$, and armchair, $T_T=a$—tubes, the translational period can get very large for chiral tubes,[3] as seen from the T_T values listed in Table II. For $\zeta\neq 0$ calculations, caution concerning the $z_{\min}$ and $z_{\max}$ values is required; we have put $z_{\max}=50$ Å$+T_T$ and retained the lower z limit ($z_{\min}=-50$ Å). We have scanned the examined (α,ζ) interval for the absolute minimum and maximum of $V_{\mathrm{NF}}^{\mathrm{discrete}}(\alpha,\beta=0,\gamma=0;\zeta)$. The differences $\Delta_{\alpha\zeta}$ between the maximum and minimum values for every tube are given as the last column in Table II. Clearly, the (α,ζ) variation is much smaller than the (β,γ) variation. We therefore conclude that the smooth-tube approach, only capturing the (β,γ) dependence, is an excellent approximation. Note that because of the weak γ dependence, one could go even further and retain only the β dependence. Indeed the x-ray scattering intensity of C_{70} molecules in SWCNT has been calculated recently by Chorro *et al.*[15] by making use of an approximate model of the C_{70} molecule: the molecular form factor is the sum of the form factors of nine circles with a linear atomic density along each circle. Our results justify this approximation. Finally we notice that with neglect of the γ dependence, Eq. (3.6) reduces to

$$\mathcal{U}_l^t(\lambda_t;\beta)=\alpha_l^{t,0}(\lambda_t)P_l(\cos\beta), \tag{4.1}$$

where $P_l(\cos\beta)$ are Legendre polynomials.

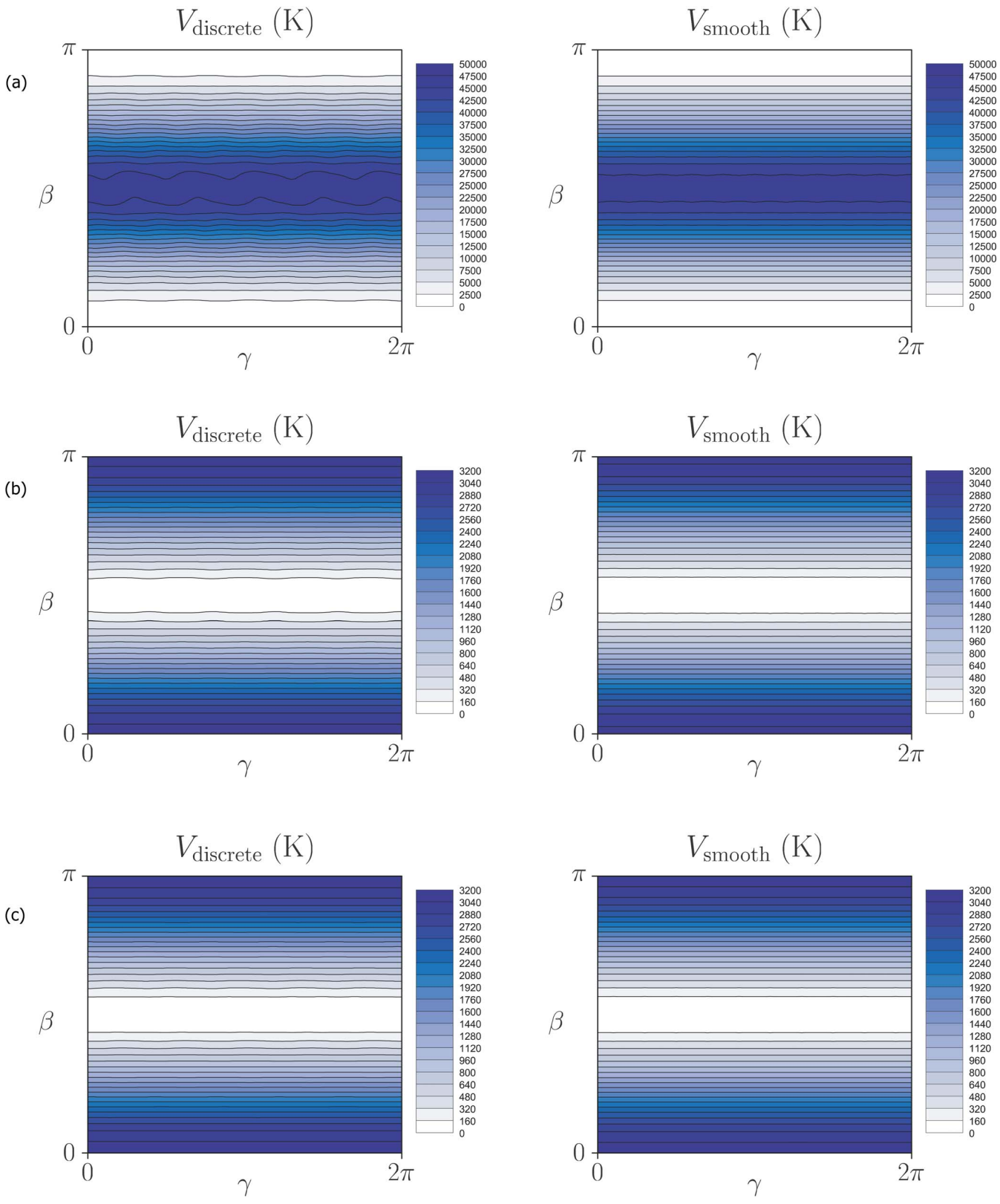

FIG. 5. (Color online) Mercator maps $V_{\mathrm{NF}}^{\mathrm{discrete}}(\alpha=0,\beta,\gamma;\zeta=0;n,m)$ (left) and $V_{\mathrm{NF}}^{\mathrm{smooth}}(\beta,\gamma;R_T)$ (right), for (a) (14, 4), (b) (19, 0) and (c) (11, 11) tubes. The absolute minima have been subtracted.

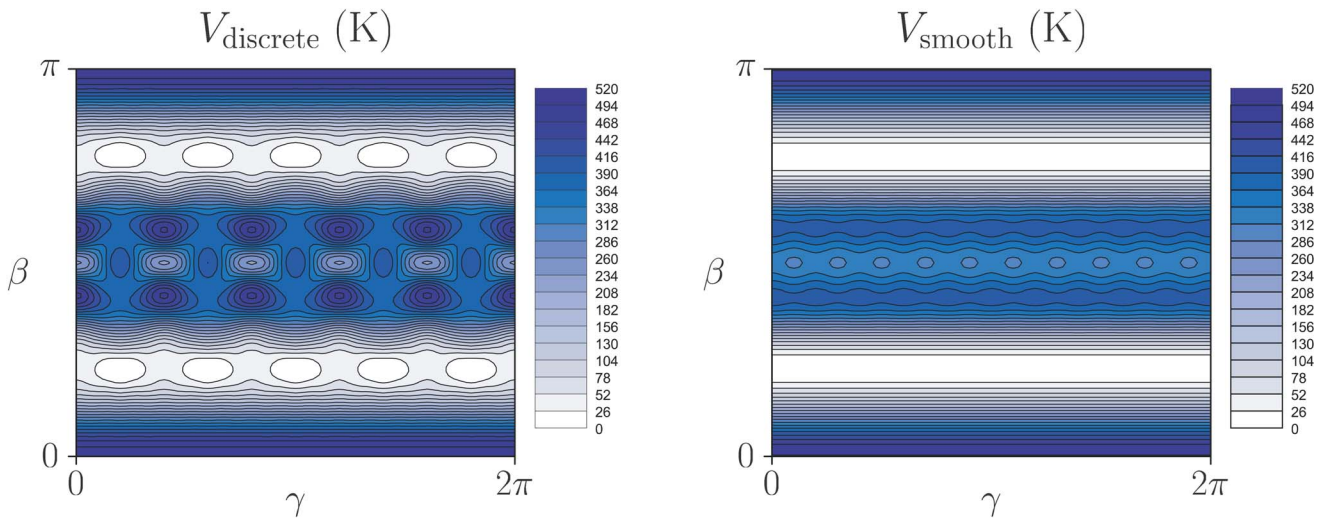

FIG. 6. (Color online) Mercator maps $V_{\text{NF}}^{\text{discrete}}(\alpha=0,\beta,\gamma;\zeta=0;n,m)$ (left) and $V_{\text{NF}}^{\text{smooth}}(\beta,\gamma;R_{\text{T}})$ (right) for a (18, 0) tube. The absolute minima have been subtracted.

V. LYING AND STANDING MOLECULAR ORIENTATIONS: OFF-AXIS POSITIONS

The Mercator maps of Figs. 5 and 6 show three different regimes. In Fig. 5(a), for a tube with radius R_T=6.49 Å, the potential $V_{\text{NF}}^{\text{smooth}}(\beta,\gamma)$ has its minimum at β=0, meaning that the molecule's long axis is aligned with the tube axis (z axis). In Figs. 5(b) and 5(c), R_T=7.53 and 7.55 Å, respectively, the potentials have their minima at $\beta=\pi/2$, corresponding to a molecular orientation with the long axis perpendicular to the tube axis. These respective configurations are the lying and standing orientations discussed in the Introduction [Figs. 2(a) and 2(c)]. Interestingly, an intermediate regime is seen in Fig. 6, R_T=7.13 Å, $V_{\text{NF}}^{\text{smooth}}(\beta,\gamma)$ exhibiting an energy minimum at $\beta\approx 41°$. This situation corresponds to the orientation where the C_{70} molecules's long axis is tilted away (by approximately 41°) from the tube's long axis [Fig. 2(b)].

We have examined the range 6.5 Å$\lesssim R_T \lesssim$7.35 Å in more detail by means of the smooth-tube approach—proven to be very adequate in the previous section. We have determined the β-angle yielding the minimum nanotube field $V_{\text{NF}}^{\text{smooth}}(\beta,\gamma)$—as observed above, the γ angle is of little importance—by starting from R_T=6.5 Å and incrementing with steps of 0.05 Å. The resulting β_{min} values are plotted in Fig. 7. The transition from lying to standing C_{70} molecular orientations is seen to cover the range 6.925 Å$\lesssim R_T \lesssim$7.175 Å. This range agrees well with the interval 7 Å$\lesssim R_T \lesssim$7.2 obtained in Ref. 15. In Ref. 13, the (10,10) tube with radius R_T=6.86 Å and the (11,11) tube with radius R_T=7.55 were examined both experimentally and theoretically; the former was found to contain C_{70} molecules in the lying orientation, while the latter exhibited standing C_{70} molecules. The same two tubes have been the subject of a molecular dynamics (MD) study arriving at the same conclusion[32]. In Ref. 14, the lying orientation was concluded for R_T=6.8 Å from HRTEM experiments while R_T=7.45 Å and R_T=8.05 Å tubes contain standing molecules. In Ref. 33, the (17,0) tube (R_T=6.74 Å) and the (19,0) tube (R_T=7.53 Å) were concluded [from discrete Fourier transform (DFT) calculations] to orient the molecules into lying and standing orientations, respectively. All this is in accordance with our findings (Fig. 7).

So far, the C_{70} molecule's center of mass has been restricted to lie on the tube's long axis. While this is the natural configuration for small-enough tubes (the molecule then experiences short-range repulsion), we expect the molecule to "stick" to the tube wall from some radius onwards. We address this issue by performing V_{NF} calculations where the molecule is allowed to make transversal off-center displacements. The calculations are performed within the smooth-tube approximation. Since we want to focus on the transversally translational dependence, we fix the molecule's orientation at (α=0, $\beta=\beta_0$, γ=0). Note that α dependence is now present due to the absence of cylindrical symmetry when transversal motion is allowed. We consider lying (β_0=0) as well as ($\beta_0=\pi/2$) configurations. Translations

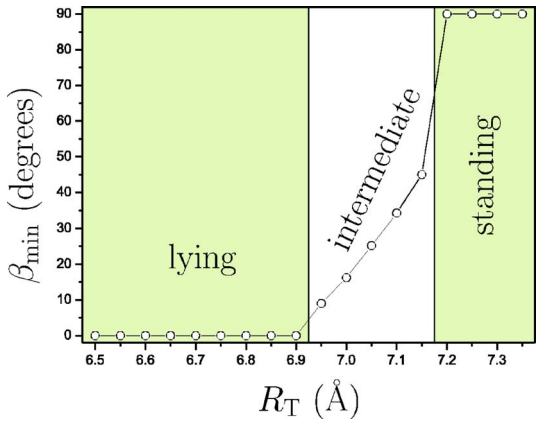

FIG. 7. (Color online) Euler angle β_{min} value at which the minimum of $V_{\text{NF}}^{\text{smooth}}(\beta_{\text{min}},\gamma)$ occurs, as a function of tube radius R_T. For $R_T\lesssim$6.925 Å, β_{min}=0, corresponding to lying molecular orientations, Fig. 2(a). For $R_T\gtrsim$7.175 Å, $\beta_{\text{min}}=\frac{\pi}{2}$, corresponding to the standing molecular orientation shown in Fig. 2(c). In between, $0<\beta_{\text{min}}<\frac{\pi}{2}$, corresponding to tilted molecular orientations [Fig. 2(b)].

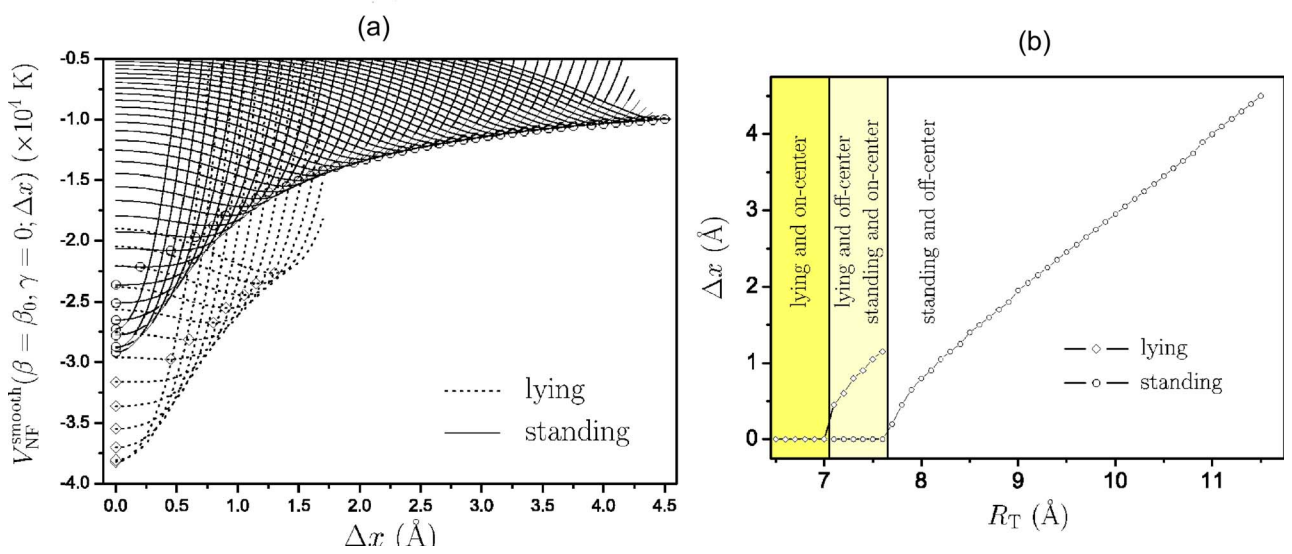

FIG. 8. (Color online) (a) Nanotube field $V_{NF}^{smooth}(\beta=\beta_0, \gamma=0; \Delta x)$, for lying ($\beta_0=0$, dotted lines) and standing ($\beta_0=\pi/2$, solid lines) C_{70} molecular orientations, as a function of the displacement Δx. For the lying orientation, curves for the radii $R_T=6.5, 7.6, \ldots, 7.7$ Å are shown, the minima are marked by diamonds. For the standing orientation, curves for the radii $R_T=6.9, 7.0, \ldots, 11.5$ Å are plotted, minima are marked by circles. (b) Minimum location as a function of the tube radius, for lying (diamonds, $\Delta x=0$) and standing (circles, $\Delta x>0$) molecules (some points have been omitted to avoid overlapping). Three regimes can be distinguished.

along the x axis are taken into account; we denote the off-center displacements by Δx, $\Delta x=0$ corresponds to the on-axis position. From the observations made in the previous section we argue that any α, γ, or ζ dependence is small. The expansion in SARFs, Eq. (3.5), cannot be used here since the cylindrical symmetry is broken for $\Delta x \neq 0$. One needs to work with explicit Euler rotation coordinate transforms as indicated in the Appendix.

In Fig. 8, two sets of fields $V_{NF}^{smooth}(\beta=\beta_0, \gamma=0; \Delta x)$ are plotted as a function of Δx. The first set shows the nanotube field values for molecules in the lying orientation ($\beta_0=0$), for the radii $R_T=6.5, 6.6, \ldots, 7.7$ Å. The energy minimum starts to differ from zero from $R_T \approx 7.05$ Å. The second set assumes the molecule to be in the standing orientation ($\beta_0=\pi/2$), and shows the results for the radii $R_T=6.9, 7.0, \ldots, 11.5$ Å. An off-center position starts to be favorable when $R_T \approx 7.65$ Å. Comparing absolute values, we see that for 7.05 Å $\lesssim R_T \lesssim$ 7.25 Å, the situation "lying and off-center" is preferred to "standing and on-center." For the range 7.25 Å $\lesssim R_T \lesssim$ 7.65 Å, "standing and on-center" is energetically more favorable than "lying and off-center." The MD results of Troche *et al.*[32] predict off-center arrangements for the (12,12) tube ($R_T=8.24$ Å) while the (11,11) tube ($R_T=7.55$ Å) contains on-axis (standing) molecules, in agreement with our regimes.

We conclude that for both lying and standing molecular orientations, actual tube radius intervals exist for which the molecules are confined onto the encapsulating nanotube's long axis. For these cases, chains of C_{70} molecules—i.e., peapod systems $(C_{70})_N$@SWCNT—will be studied in the next section.

VI. CHAINS OF TRANSVERSALLY CONFINED C_{70} MOLECULES

We now turn our attention to $(C_{70})_N$@SWCNT peapods. Every C_{70} molecule of a peapod has a nanotube field energy V_{NF}, generally depending on the molecular position, the molecular orientation, and the tube characteristics, as described in the preceding sections. In the following we investigate properties resulting from interactions between neighboring molecules, subject to their nanotube fields, thereby proceeding along the lines of Refs. 17 and 18.

We assume the chain of encapsulated C_{70} molecules to be confined onto the nanotube's long axis—a physical realization of a 1D system. From the previous sections we expect such transversal confinement to be the case for lying molecules when the tube radius is sufficiently small, $R_T \lesssim 7.05$ Å, and for standing molecules when 7.3 Å $\lesssim R_T \lesssim 7.6$ Å. When studying C_{70}-C_{70} interactions, only longitudinal molecular displacements then remain as translational degrees of freedom. We label the N C_{70} molecules by an index $n=1, \ldots, N$ and their center-of-mass positions by $\boldsymbol{\zeta}(n)=\zeta(n)\mathbf{e}_z$, with $\mathbf{e}_z$ the unit vector along the z axis. For the equilibrium (center of mass to center of mass) distance between two neighboring C_{70} molecules we write a, so that at equilibrium, $\zeta(n)=na$.

As seen in the previous sections, the smooth-tube approximation is justified when describing the interaction between a transversally confined C_{70} molecule and the surrounding tube. Within the smooth-tube approach, cylindrical symmetry makes the final Euler rotation of the C_{70} molecules (over $-\alpha$ about the z axis) irrelevant. Fixing the Euler angles β and γ at their values corresponding to the energy minimum ($\beta=0$ and $\gamma=0$ for lying molecules, $\beta=\pi/2$ and $\gamma=0$ for standing molecules), only α remains as an orientational degree of freedom, which we redefine, for the nth molecule, as $\psi(n)$.

The interaction energy of two neighboring C_{70} molecules can therefore formally be written as

TABLE III. Additional potential constants C_1, C_2, and B, required for modelling C_{70}–C_{70} interactions, taken from Ref. 24.

tt'	DD	DI	II
$C_1^{tt'}$ ($\times 10^6$ K)	6.24	0.84	0.114
$C_2^{tt'}$ (Å^{-1})	3.2	3.3	3.4
$B^{tt'}$ (K Å^6)	0	0	0

$$U(n,n+1) \equiv U[\zeta(n+1)-\zeta(n);\psi(n+1)-\psi(n)]. \tag{6.1}$$

Obviously, the energy depends only explicitly on the differences in translational and orientational variables. We emphasize that the role of the nanotube field is to confine the molecules (i) onto the tube axis, so that only the longitudinal displacive degree of freedom $\zeta(n)$ remains, and (ii) orientationally, so that only a rotation over $\psi(n)$ about the z axis is possible.

We continue to treat a C_{70} molecules as the rigid cluster of ICs described above, following earlier theoretical work on C_{70}-C_{70} interactions in solid C_{70}[23]. Whereas before, when modelling the C_{70}-tube interaction, we had only a-a, D-a, and I-a interactions [see Eq. (2.3)], we now have D-D, D-I, and I-I interactions as well:

$$U(n,n+1) = \sum_{t=a,D,I} \sum_{t'=a,D,I} \sum_{\Lambda_t=1}^{N_t} \sum_{\Lambda_{t'}=1}^{N_{t'}} v^{tt'}(|\mathbf{r}_{\Lambda_{t'}} - \mathbf{r}_{\Lambda_t}|), \tag{6.2a}$$

with the Born–Mayer–van der Waals potentials now reading

$$v^{tt'}(r) = C_1^{tt'} e^{-C_2^{tt'} r} - \frac{B^{tt'}}{r^6}. \tag{6.2b}$$

The additional potential constants are listed in Table III.

As described in detail in Ref. 18, the total interaction Hamiltonian

$$V = \sum_{n=1}^{N-1} U(n,n+1) \tag{6.3}$$

can be written as

$$V = (N-1)J_0 + V^{\mathrm{RR}} + V^{\mathrm{TT}} + V^{\mathrm{RRT}} + \ldots, \tag{6.4}$$

the result of expanding $U(n,n+1)$ in a Taylor series with respect to $\zeta(n+1)-\zeta(n)$ and then expanding the Taylor coefficients in Fourier series with respect to $\psi(n+1)-\psi(n)$.

The rotation-rotation (RR) term V^{RR} in Eq. (6.4) relates to the zeroth-order Taylor expansion term

$$U[\zeta(n+1)-\zeta(n)=a;\psi(n+1)-\psi(n)] = \sum_{l=0}^{\infty} J_l \cos\{l[\psi(n+1)-\psi(n)]\}, \tag{6.5}$$

which contains only cosine terms due to the invariance of $U(n+1,n)$ when replacing $\Delta\psi \equiv \psi(n+1)-\psi(n)$ by $-\Delta\psi$. For lying molecules, fivefold rotation symmetry (about the z axis) implies the vanishing of terms with $l \neq 0,5,10,\ldots$, while for standing molecules, one has twofold symmetry about the z axis, so that only $l=0,2,4,\ldots$ terms are nonvanishing in expansion (6.5). Omitting the constant term, written separately as the first term in the right-hand side (RHS) of Eq. (6.4), one has up to leading order

$$V^{\mathrm{RR}} = \sum_{n=1}^{N-1} U[\zeta(n+1)-\zeta(n)=a;\psi(n+1)-\psi(n)] \approx \sum_{n=1}^{N-1} J_s \cos\{s[\psi(n+1)-\psi(n)]\}, \tag{6.6a}$$

with

$$J_s = \frac{1}{\pi}\int_0^{2\pi} d\psi \cos(s\psi) \tag{6.6b}$$

with $s=5$ for lying and $s=2$ for standing molecules, respectively. Introducing the definition

$$\mathbf{S}(n) \equiv \begin{pmatrix} \cos[s\psi(n)] \\ \sin[s\psi(n)] \end{pmatrix}, \tag{6.7}$$

V^{RR} can be rewritten as the Hamiltonian of a rotor model with O_2 symmetry:[34]

$$V^{\mathrm{RR}} = J_s \sum_{n=1}^{N-1} \mathbf{S}(n+1)\cdot\mathbf{S}(n). \tag{6.8}$$

The rotation-rotation-translation (RRT) term V^{RRT} in Eq. (6.4) involves the first-order Taylor expansion coefficient

$$U'[\zeta(n+1)-\zeta(n);\psi(n+1)-\psi(n)] = \sum_{l=0}^{\infty} J'_l \cos\{l[\psi(n+1)-\psi(n)]\} \approx J'_0 + J'_s \cos\{s[\psi(n+1)-\psi(n)]\}, \tag{6.9a}$$

with

$$J'_0 = \frac{1}{2\pi}\int_0^{2\pi} d\psi \left.\frac{\partial U[\zeta(n+1)-\zeta(n);\psi]}{\partial[\zeta(n+1)-\zeta(n)]}\right|_{\zeta(n+1)-\zeta(n)=a}, \tag{6.9b}$$

$$J'_s = \frac{1}{\pi}\int_0^{2\pi} d\psi \cos(s\psi) \left.\frac{\partial U[\zeta(n+1)-\zeta(n);\psi]}{\partial[\zeta(n+1)-\zeta(n)]}\right|_{\zeta(n+1)-\zeta(n)=a}. \tag{6.9c}$$

Performing the lattice sum gives

$$V^{\mathrm{RRT}} = J'_s \sum_{n=1}^{N-1} \mathbf{S}(n+1)\cdot\mathbf{S}(n)[\zeta(n+1)-\zeta(n)-a]. \tag{6.10}$$

The equilibrium lattice constant a is determined by the condition

$$J'_0(a) = 0. \tag{6.11}$$

TABLE IV. Equilibrium lattice constant a (units Å), Fourier expansion coefficients J_s, J_s', and J_0'' (respective units K, K Å^{-1}, and K Å^{-2}), and lattice contractions δa (units Å) for a few temperatures T (units K). Lying and standing molecules have $s=5$ and $s=2$, respectively.

					δa (Å)		
	a (Å)	J_s (K)	J_s' (K Å^{-1})	J_0'' (K Å^{-2})	$T=300$ K	$T=10$ K	$T=1$ K
Lying ($s=5$)	11.034	13.67	−63.14	9497.64	0.000151	0.00373	0.00640
Standing ($s=2$)	9.761	−54.88	176.55	11823.75	0.00136	0.0135	0.0148

Finally, the translation-translation term V^{TT} in the RHS side of Eq. (6.4) follows from the constant Fourier term of the second order Taylor expansion coefficient

$$U''[\zeta(n+1)-\zeta(n);\psi(n+1)-\psi(n)] = \sum_{l=0}^{\infty} J_l'' \cos\{l[\psi(n+1)-\psi(n)]\} \approx J_0'', \quad (6.12a)$$

with

$$J_0'' = \frac{1}{2\pi}\int_0^{2\pi} d\psi \left.\frac{\partial^2 U[\zeta(n+1)-\zeta(n);\psi]}{\partial[\zeta(n+1)-\zeta(n)]^2}\right|_{\zeta(n+1)-\zeta(n)=a}. \quad (6.12b)$$

The TT term reads

$$V^{\mathrm{TT}} = \frac{J_0''}{2}\sum_{n=1}^{N-1}[\zeta(n+1)-\zeta(n)-a]^2, \quad (6.13)$$

the Hamiltonian of a chain of particles connected by harmonic springs.

In Table IV we have collected the values of the parameters a, J_s, J_s', and J_0'', all resulting from the intermolecular potential set up by Eqs. (6.2a) and (6.2b) and the potential constants of Tables I and III. Our equilibrium a values agree very well with the most recent experimental values $a=11.0$ Å (lying) and $a=9.8$ Å (standing),[15] and with values obtained by DFT calculations[33] ($a=11.1$ Å, lying, and $a=9.9$ Å, standing).

For lying molecules, $J_{s=5}>0$, implying minimal RR energy when $\Delta\psi=36°$, i.e., when neighboring molecules have periodically shifted orientation angles. We point out that the facing pentagons of neighboring molecules are then in a staggered configuration. For standing molecules, $J_{s=2}<0$, so that the RR energy is minimal when $\Delta\psi=0°$, i.e., when the long ellipsoidal axes of neighboring molecules are parallel to each other (and perpendicular to the z axis). This is consistent with the Lennard-Jones (based on Ref. 35) model of Chorro *et al.*,[15] who obtained $\Delta\psi=0°$ at the equilibrium a value as well.[36]

Having established expressions for the various terms of the lattice Hamiltonian V, Eq. (6.4), temperature-dependent properties can be studied. The starting point is the nearest-neighbor orientational correlation $\Gamma(1)$, defined as the classical thermal average

$$\Gamma(1) = \langle \mathbf{S}(n+1)\cdot\mathbf{S}(n)\rangle. \quad (6.14)$$

A classical calculation is justified up to temperatures as low as $T\approx 0.01$ K because of a C_{70} molecule's large moments of inertia.[37] The thermal average in Eq. (6.14) is calculated for equilibrium lattice positions, i.e., for $V=V^{\mathrm{RR}}$—the constant term $(N-1)J_0$ is irrelevant. The analytically exact result[17,18]

$$\Gamma(1) = \frac{I_1\left(-\frac{J_s}{T}\right)}{I_0\left(-\frac{J_s}{T}\right)}, \quad (6.15)$$

where I_0 and I_1 are modified Bessel functions of the first kind, is known from the O_2 rotor model[38]. Note that throughout the paper, energies like J_s are in units K. For $T\to\infty$, $\Gamma(1)\to 0$, meaning no orientational ordering. The low T limit $T\to 0$ gives $\Gamma(1)\to 1$, implying perfect long-range orientational order. At finite temperatures, short-range orientational correlations interfere with translational correlations. Replacing $\mathbf{S}(n+1)\cdot\mathbf{S}(n)$ in expression (6.10) by its thermal average $\Gamma(1)$ one obtains the result

$$\langle\zeta(n+1)-\zeta(n)\rangle = a - \frac{J_s'\Gamma(1)}{J_0''}. \quad (6.16)$$

The term $-\delta a \equiv -J_s'\Gamma(1)/J_0''$ is a consequence of the presence of the V^{RRT} term. In the regime of lying molecules ($s=5$), $J_5'<0$, $\Gamma(1)<0$, and $J_0''>0$, so that $\delta a>0$. For standing molecules ($s=2$), J_2', $\Gamma(1)$, and J_0'' are all positive, implying $\delta a>0$ as well. Hence, for both cases, RRT leads to a reduction of the average distance a between neighboring C_{70} molecules with decreasing temperature. In Table IV we have written down the values of δa for a few temperatures. This type of contraction has been called an effect of torsio-thermo mechanics[18], after the analogy with the phenomenon of magneto-thermo mechanics seen in compressible magnets[39]. Kataura *et al.*[11] and Maniwa *et al.*[12] have given an experimental report on the thermal expansion (with increasing temperature) of the intermolecular spacing for both the lying and standing arrangements. They observed a substantially larger expansion of the intermolecular distance for the standing than for the lying configuration, a result in agreement with our findings: assuming a simple linear relation of the form $\Delta a/a=\alpha\Delta T$, we obtain, using the $T=300$ K and $T=1$ K values of Table IV, thermal expansion coefficients $\alpha\approx 2.1\times 10^{-5}$ K^{-1} and $\alpha\approx 4.5\times 10^{-5}$ K^{-1} for lying and standing molecules, respectively. The latter value is not too discrepant

from the value $\sim 11 \times 10^{-5}$ K^{-1} estimated by Maniwa *et al.*[12] (based on the interval 300 K$\leqslant T \leqslant$999 K).

Concerning the relative orientation angle $\Delta\psi$ of neighboring standing molecules, Chorro *et al.*[15] pointed out that the energy variation when varying $\Delta\psi$ is small ($\sim$0.01 eV $\approx$116 K at the equilibrium a value for their Lennard-Jones model) and that at room temperature the molecules will exhibit more-or-less independent molecular orientation angles $\psi(n)$. While we have a similar RR energy range ($2J_{s=2} \approx 110$ K), orientational correlation $\Gamma(1)$ values show that already at 100 K, significant correlation occurs [$\Gamma(1)=0.26$]. [For lying molecules, $\Gamma(1)=0.26$ at $T=25$ K.] We therefore suggest that sub-100 K experiments might reveal (almost) fixed relative molecular orientations ($\Delta\psi=0°$, long ellipsoidal axes of neighboring molecules parallel to each other).

Although our 1D model does not exhibit translational long-range order (i.e., resembles a 1D liquid) and does therefore not lead to a diffraction pattern of ideal Bragg peaks, we have shown in Refs. 17 and 18 that the structure factor $S(q)$ for the center-of-mass positions of the 1D chain does have clearly discernible resonances in reciprocal space. The result

$$S(q) = \frac{1 - Z^2(q)}{1 + Z^2(q) - 2Z(q)\cos(q\langle\zeta(n+1) - \zeta(n-1)\rangle)} \tag{6.17}$$

is a generalization of a similar expression derived by Emery and Axe[40] for a chain of mercury atoms in $Hg_{3-\delta}AsF_6$. In Eq. (6.17) we have defined

$$Z(q) = e^{-(q^2T^2/2J_0'')}, \tag{6.18}$$

and $\langle\zeta(n+1)-\zeta(n)\rangle$ is given by Eq. (6.16). Still at $T=300$ K, the structure factor $S(q)$ exhibits narrow peaks, centered around $q_j = j(2\pi/\langle\zeta(n+1)-\zeta(n)\rangle)$, $j \in \mathbb{Z}$. They appear as streaks in the experimental diffraction pattern.[9,11]

VII. CONCLUSIONS

Knowledge of the potential energy of a C_{70} molecule encapsulated in a SWCNT, due to van der Waals interactions, allows the theoretical determination of experimentally observable configurations. We have performed interaction energy calculations by means of two approaches. The first, atomistic, description takes the precise structure (network of carbon atoms) of the SWCNT into account. The C_{70} is taken as a cluster of ICs (atoms, D and I centers). The interaction energy—called the molecule's nanotube field—is then obtained as a direct summation of Born–Mayer–van der Waals pair potentials. It depends on six variables: three Euler angles α, β, and γ, a longitudinal coordinate ζ, and the SWCNT indices n and m. In the second description—the smooth-tube approximation—the SWCNT is modeled as a continuous carbonic surface density with cylindrical symmetry while the C_{70} cluster model is retained. This not only reduces the number of variables (only β, γ, and the tube radius R_T remain) but it allows the expansion of the nanotube field in SARFs. Apart from resulting in mathematical-physical clarity (symmetry and pair potential characteristics are separated), calculations are seriously sped up in this way. The nanotube field's β and γ dependences can be drawn conveniently as Mercator maps[31]. Upon comparing the nanotube fields obtained via the atomistic and the continuous approach, we see that the latter works very well and thus provides an adequate approximation for nanotube field calculations (Figs. 5 and 6). Also, we notice limited γ dependence, which can be understood from an examination of the SARFs expansion wherein γ-dependent terms start to enter from $l=10$ multipole moments onwards only.

As intuitively expected and already observed experimentally[9–15] and reproduced theoretically,[13,15,33] C_{70} molecules adopt a lying orientation for small and a standing orientation for large tube radii. We have performed nanotube field calculations (within the smooth-tube approximation) for a whole range of R_T values and arrive at the following result. For $R_T \lesssim 6.925$ Å, lying molecules are energetically most favorable. For $R_T \gtrsim 7.175$ Å, the standing orientation is recovered. In between, we have an intermediate regime where the angle β changes gradually from 0° to 90° (see Fig. 7). The x-ray diffraction experiments of Chorro *et al.*[15] lead to a transition radius of $R_T=7.1$ Å, falling nicely in our intermediate region, and their Lennard-Jones calculations[15] also predicted an intermediate region (7.0 Å$\leqslant R_T \leqslant$7.2 Å) agreeing well with our values. The slightly lower value $R_T \approx 6.95$ Å as the transition radius has been suggested in Ref. 41 to account for Raman spectroscopy measurements on double-walled CNTs synthesized by heating $(C_{70})_N$@SWCNT peapods.

A C_{70} molecule will occupy an on-axis position only for small-enough tube radii; from some radius onwards, the attractive van der Waals forces will make the molecule stick to the tube wall. We have investigated the energies for off-axis positions for both lying and standing C_{70} molecules. Four regimes can be distinguished (Fig. 8). For $R_T \lesssim 7.05$ Å, lying on-axis molecules are energetically most favorable. For 7.05 Å$\lesssim R_T \lesssim$7.25 Å, lying but off-axis molecules minimize the energy. For $R_T \gtrsim 7.25$ Å standing configurations are favored, on-axis for 7.25 Å$\lesssim R_T \lesssim$7.65 Å and off-axis for $R_T \gtrsim 7.65$ Å.

Finally, we have applied our nanotube field results to $(C_{70})_N$@SWCNT peapods. The nanotube field acts on every encapsulated C_{70} molecule as a confinement potential; its degrees of freedom are reduced to one rotational and one translational degree of freedom (rotation about and translation along the tube's long axis, respectively). This is a realistic picture for tube radii $R_T \lesssim 7.05$ Å and 7.25 Å$\lesssim R_T \lesssim$7.65 Å, featuring on-axis lying and standing molecules, respectively. The interaction between two nearest-neighbor molecules depends only on their relative orientation angle. Therefore, these 1D chains of confined C_{70} molecules are physical realizations of the O_2 rotor model[38]. We find that the equilibrium intermolecular distances a agree well with experimental values[15] for both the lying and the standing regime. Orientational nearest-neighbor correlations $\Gamma(1)$ are small at room temperature but start to be non-negligible below, say, $T=100$ K for standing molecules. Due to RRT coupling we observe a lattice contraction with decreasing temperature. This effect is very small, however: at $T=1$ K the predicted contraction is still of the order of $\sim$0.01 Å only. Pseudo-Bragg peaks associated with the 1D chains of C_{70}

molecules are already clearly present at room temperature, though, as seen from the expression for the translational structure factor $S(q)$. The 1D character of a $(C_{70})_N$ peapod system was stressed by Maniwa *et al.*[12] since they observed a continuous change in the lattice parameter a rather than a phase transition—orientational ordering accompanied by a jump in the lattice constant a—at some temperature. Thus, the O_2 rotor model[38] is an apt description for $(C_{70})_N$ peapods where the C_{70} molecules are confined onto the tube axis. In the case of off-axis positions, complex stacking patterns (e.g., helices) are possible as discussed in Ref. 32.

In summary, we have shown that the smooth-tube approximation works very well for $(C_{70})_N$@SWCNT peapods, and that it can be used as a means for theoretically studying single-molecule properties (lying or standing orientations, on- or off-axis positions), as well as many-molecule properties (orientational correlations, 1D liquid behavior). In particular, it could be used when developing scattering intensity formulas—as in Ref. 15 for x-ray diffraction—for future comparison with experiment.

ACKNOWLEDGMENTS

We thank P. Launois for communicating results[15] to us prior to publication. B.V. acknowledges the Fonds voor Wetenschappelijk Onderzoek—Vlaanderen.

APPENDIX: SYMMETRY-ADAPTED ROTATOR FUNCTIONS EXPANSION

In this appendix we derive Eq. (3.5) which stands for the expansion of the potential in terms of SARFs. We start from Eq. (3.4). The distance $|\boldsymbol{\rho}-\mathbf{r}_{\Lambda_t}|$ can be written as

$$|\boldsymbol{\rho}-\mathbf{r}_{\Lambda_t}| = \{R_T^2 + r_{\Lambda_t}^2 \sin^2\theta_{\Lambda_t} - 2R_T r_{\Lambda_t}\cos(\Phi-\phi_{\Lambda_t})\sin\theta_{\Lambda_t} + Z^2 + r_{\Lambda_t}^2\cos^2\theta_{\Lambda_t} - 2Zr_{\Lambda_t}\cos\theta_{\Lambda_t}\}^{1/2}, \tag{A1}$$

where $(r_{\Lambda_t},\theta_{\Lambda_t},\phi_{\Lambda_t})$ are spherical coordinates:

$$x_{\Lambda_t} = r_{\Lambda_t}\sin\theta_{\Lambda_t}\cos\phi_{\Lambda_t}, \tag{A2a}$$

$$y_{\Lambda_t} = r_{\Lambda_t}\sin\theta_{\Lambda_t}\sin\phi_{\Lambda_t}, \tag{A2b}$$

$$z_{\Lambda_t} = r_{\Lambda_t}\cos\theta_{\Lambda_t}. \tag{A2c}$$

The Cartesian and spherical IC coordinates $(x_{\Lambda_t},y_{\Lambda_t},z_{\Lambda_t})$ and $(r_{\Lambda_t},\theta_{\Lambda_t},\phi_{\Lambda_t})$ are understood to correspond to the C_{70} molecule's standard orientation.

1. Molecular layer structure

The dependence of $V_{\mathrm{NF}}^{\mathrm{smooth}}$ on the Euler angles α, β, and γ might be formulated by explicitly performing the appropriate coordinate transforms and insert the transformed coordinates, say $(x'_{\Lambda_t},y'_{\Lambda_t},z'_{\Lambda_t})$, into Eq. (A1), which is then inserted into Eq. (3.4). For the off-center calculations described in Sec. V this is how one has to proceed. When cylindrical symmetry is present, an expansion in SARFs is another—more advantageous—route, however, for which only the standard orientation coordinates are required. The atoms and the other ICs of a C_{70} molecule in standard orientation should be thought of as being grouped in "layers," as in Ref. 29. The layer classification is based on the ICs' z coordinates: ICs of the same type having the same z_{Λ_t} value (we recall that the z axis coincides with the tube's long cylindrical axis) constitute a layer. Layers can be seen as planes perpendicular to the z axis containing 5 or 10 ICs. We label them by the index λ_t. Within each layer, the ICs are labeled by the index ν_t, so that

$$\Lambda_t \equiv (\lambda_t,\nu_t). \tag{A3}$$

By construction, the radial coordinates r_{Λ_t} are equal for ICs of a same layer, $r_{\Lambda_t}\equiv r_{\lambda_t}$, and likewise for the polar angles θ_{Λ_t}, $\theta_{\Lambda_t}\equiv\theta_{\lambda_t}$. Only the azimuthal angles ϕ_{Λ_t} are truly ν_t-dependent: $\phi_{\Lambda_t}\equiv\phi_{\lambda_t,\nu_t}$. Since ϕ_{λ_t,ν_t} occurs only in the difference $\Phi-\phi_{\lambda_t,\nu_t}$ in Eq. (A1), it may be dropped when inserting expression (A1) into Eq. (3.4):

$$V_{\mathrm{NF}}^{\mathrm{smooth}}(R_T) = \sigma R_T \sum_t \sum_{\Lambda_t} \int_0^{2\pi} d\Phi \int_{z_{\min}}^{z_{\max}} dZ \tilde{v}^t(R_T,r_{\lambda_t},\theta_{\lambda_t},\Phi,Z), \tag{A4a}$$

$$\tilde{v}^t(R_T,r_{\lambda_t},\theta_{\lambda_t},\Phi,Z) \equiv v^t(\{R_T^2 + r_{\lambda_t}^2\sin^2\theta_{\lambda_t} - 2R_T r_{\lambda_t}\cos\Phi\sin\theta_{\lambda_t} + Z^2 + r_{\lambda_t}^2\cos^2\theta_{\lambda_t} - 2Zr_{\lambda_t}\cos\theta_{\lambda_t}\}^{1/2}). \tag{A4b}$$

Here we have replaced the infinite integration boundaries by the finite values $z_{\min}$ and $z_{\max}$.

2. Symmetry-adapted rotator functions (SARFs)

We continue by expanding $\tilde{v}^t(R_T,r_{\lambda_t},\theta_{\lambda_t},\Phi,Z)$, Eq. (A4b), in $m=0$ spherical harmonics:

$$\tilde{v}^t(R_T,r_{\lambda_t},\theta_{\lambda_t},\Phi,Z) = \sum_{l=0,2,4,\ldots} \tilde{v}_l^t(R_T,r_{\lambda_t},\Phi,Z)Y_l^{m=0}(\theta_{\lambda_t}), \tag{A5a}$$

$$\tilde{v}_l^t(R_T,r_{\lambda_t},\Phi,Z) = 2\pi\int_0^{\pi}\sin\theta d\theta \tilde{v}^t(R_T,r_{\lambda_t},\theta_{\lambda_t},\Phi,Z)Y_l^{m=0}(\cos\theta). \tag{A5b}$$

Inversion symmetry of the smooth tube implies that only coefficients $\tilde{v}_l^t$ with l even are different from zero. Here, the spherical harmonics of Ref. 20 are understood. Defining

$$\tilde{v}_l^t(R_T,\lambda_t) = \int_0^{2\pi} d\Phi \int_{-\infty}^{+\infty} dZ \tilde{v}_l^t(R_T,r_{\lambda_t},\Phi,Z) \tag{A6}$$

allows to rewrite Eq. (A4a) as

$$V_{\mathrm{NF}}^{\mathrm{smooth}}(R_T) = \sigma R_T \sum_t \sum_{\lambda_t} \sum_{\nu_t} \sum_{l=0}^{\infty} \tilde{v}_l^t(R_T,\lambda_t) Y_l^{m=0}(\theta_{\lambda_t}). \tag{A7}$$

We recall that up to now, the C_{70} molecule has been assumed to be in the standard orientation—the (spherical) IC coordinates $(r_{\Lambda_t}, \theta_{\Lambda_t}, \phi_{\Lambda_t})$ refer to the standard orientation. We now consider arbitrary orientations and let the Euler rotations operator $\mathcal{R}(\alpha,\beta,\gamma)$ transform $V_{\mathrm{NF}}^{\mathrm{smooth}}$:

$$\begin{aligned} V_{\mathrm{NF}}^{\mathrm{smooth}}(\alpha,\beta,\gamma;R_T) &\equiv \mathcal{R}(\alpha,\beta,\gamma) V_{\mathrm{NF}}^{\mathrm{smooth}}(R_T) \\ &= \sigma R_T \sum_t \sum_{\lambda_t} \sum_{\nu_t} \sum_{l=0}^{\infty} \tilde{v}_l^t(R_T,\lambda_t) \\ &\quad \times \mathcal{R}(\alpha,\beta,\gamma) Y_l^{m=0}(\theta_{\lambda_t}). \end{aligned} \tag{A8}$$

Following the convention of Ref. 20, a coordinate function $f[\mathbf{r}=(x,y,z)]$ is transformed as $\mathcal{R}(\alpha,\beta,\gamma) f(\mathbf{r}) = f[\mathcal{R}^{-1}(\alpha,\beta,\gamma)\mathbf{r}]$, where $\mathcal{R}(\alpha,\beta,\gamma) = \mathcal{R}_z(\gamma)\mathcal{R}_y(\beta)\mathcal{R}_z(\alpha)$ stands for the succesion of a rotation over $0 \leqslant \alpha < 2\pi$ about the z axis, a rotation over $0 \leqslant \beta \leqslant \pi$ about the y axis, and a rotation over $0 \leqslant \gamma < 2\pi$ about the z axis again. The x, y, and z axes are kept fixed. Note that the *coordinate transform* associated with the Euler angles reads $\mathbf{r}' = \mathcal{R}^{-1}(\alpha,\beta,\gamma)\mathbf{r} = \mathcal{R}_z(-\alpha)\mathcal{R}_y(-\beta)\mathcal{R}_z(-\gamma)\mathbf{r}$ and that the rotation of the C_{70} molecule over $-\alpha$ about the z axis is performed last. The effect of $\mathcal{R}(\alpha,\beta,\gamma)$ on spherical harmonics is described in Ref. 20:

$$\mathcal{R}(\alpha,\beta,\gamma) Y_l^{m=0}(\theta_{\lambda_t}) = \sum_{n=-l}^{l} \mathcal{D}_{n,m=0}^l(\alpha,\beta,\gamma) Y_l^n(\theta_{\lambda_t}, \phi_{\lambda_t,\nu_t}), \tag{A9}$$

where $\mathcal{D}_{n,m}^l(\alpha,\beta,\gamma)$ are Wigner $\mathcal{D}$ functions.[19] For $m=0$, Wigner $\mathcal{D}$ functions are independent of α. This is consistent with the cylindrical symmetry: indeed, a final rotation of the molecule about the z axis (over $-\alpha$) does not change its potential energy. Wigner $\mathcal{D}$ functions with $m=0$ read

$$\mathcal{D}_{n,m=0}^l(\beta,\gamma) = \sqrt{\frac{4\pi}{2l+1}} [Y_l^n(\beta,\gamma)]^*. \tag{A10}$$

In order to obtain a multipole expansion of the IC distribution in the molecule we introduce

$$c_l^{t,n}(\lambda_t) = \sum_{\nu_t} Y_l^n(\theta_{\lambda_t}, \phi_{\lambda_t,\nu_t}), \tag{A11a}$$

with the "molecular form factors"

$$g_l^t(\lambda_t) = \sqrt{\sum_{n=-l}^{l} [c_l^{t,n}(\lambda_t)]^2}. \tag{A11b}$$

Defining the multipole coefficients

$$\alpha_l^{t,n}(\lambda_t) = \frac{c_l^{t,n}(\lambda_t)}{g_l^t(\lambda_t)} \tag{A11c}$$

we rewrite $V_{\mathrm{NF}}^{\mathrm{smooth}}$ as

TABLE V. Layers, labeled λ_t, $t=a,D,I$, are sets of ICs with equal r_{λ_t} coordinates, containing $n_{\lambda_t}=10$ or 20 ICs. Compare with Fig. 4.

	n_{λ_t}	r_{λ_t} (Å)
$\lambda_a=1$	1×10	3.563
$\lambda_a=2$	2×10	3.668
$\lambda_a=3$	2×10	3.887
$\lambda_a=4$	2×5	4.012
$\lambda_a=5$	2×5	4.176
$\lambda_D=1$	2×5	3.824
$\lambda_D=2$	2×5	4.037
$\lambda_I=1$	2×10	3.546
$\lambda_I=2$	2×5	3.599

$$V_{\mathrm{NF}}^{\mathrm{smooth}}(\beta,\gamma;R_T) = \sigma R_T \sum_t \sum_{\lambda_t} \sum_{n=-l}^{l} \sum_{l=0}^{\infty} g_l^t(\lambda_t) \alpha_l^{t,n}(\lambda_t) \times \tilde{v}_l^t(R_T,\lambda_t) D_{n,m=0}^l(\beta,\gamma). \tag{A12}$$

At this point we introduce SARFs $\mathcal{U}_l^t$:

$$\mathcal{U}_l^t(\lambda_t;\beta,\gamma) = \sum_{n=-l}^{l} \alpha_l^{t,n}(\lambda_t) \mathcal{D}_{n,m=0}^l(\beta,\gamma), \tag{A13a}$$

$$V_{\mathrm{NF}}^{\mathrm{smooth}}(\beta,\gamma;R_T) = \sigma R_T \sum_t \sum_{\lambda_t} \sum_{l=0}^{\infty} g_l^t(\lambda_t) \mathcal{U}_l^t(\lambda_t;\beta,\gamma) \tilde{v}_l^t(R_T,\lambda_t). \tag{A13b}$$

Finally, we define

$$w_l^t(\lambda_t,R_T) = g_l^t(\lambda_t) \tilde{v}_l^t(R_T,\lambda_t) \tag{A14}$$

so that Eq. (3.5) is obtained:

$$V_{\mathrm{NF}}^{\mathrm{smooth}}(\beta,\gamma;R_T) = \sigma R_T \sum_t \sum_{\lambda_t} \sum_{l=0}^{\infty} w_l^t(\lambda_t,R_T) U_l^t(\lambda_t;\beta,\gamma). \tag{A15}$$

Equation (A15) is the expansion of the "smooth" nanotube field in SARFs. Note that the SARFs, given by Eq. (A13a), are layer-dependent. Interestingly, SARFs for a C_{60} molecule are not layer-dependent—see Refs. 17 and 18—a consequence of ICs of type t having the same radial coordinates $r_{\Lambda_t} \equiv r_t$.

3. Molecular layer structure revisited

Since ICs with opposite z_{Λ_t} coordinates have the same r_{Λ_t} value, the quantity $\tilde{v}_l^t(R_T,\lambda_t)$ [Eq. (A6)] is equal for layers with opposite z_{λ_t} values. We therefore redefine layers as

groups of ICs having the same $|z_{\Lambda_t}|$ value. This has an impact on the definition of $c_l^{t,n}(\lambda_t)$, Eq. (A11a), where the sum now runs over the extended number of ICs, and on the summations over λ_t now running over the newly defined set of layers. The layer structure is summarized in Table V, where some relevant layer-related values are quoted as well.

[1] S. Iijima, Nature (London) **354**, 56 (1991).
[2] M. Endo, CHEMTECH **18**, 568 (1988).
[3] R. Saito, G. Dresselhaus, and M. S. Dresselhaus, *Physical Properties of Carbon Nanotubes* (Imperial College Press, London, 1998).
[4] P. J. F. Harris, *Carbon Nanotubes and Related Structures* (Cambridge University Press, Cambridge, 1999).
[5] J. Sloan, A. I. Kirkland, J. L. Hutchison, and M. L. H. Green, Chem. Commun. (Cambridge) **2002**, 1319.
[6] M. Monthioux, Carbon **40**, 1809 (2002).
[7] B. W. Smith, M. Monthioux, and D. E. Luzzi, Nature (London) **396**, 323 (1998).
[8] H. Kataura, Y. Maniwa, T. Kodama, K. Kikuchi, K. Hirahara, K. Suenaga, S. Iijima, S. Suzuki, Y. Achiba, and W. Krätschmer, Synth. Met. **121**, 1995 (2001).
[9] K. Hirahara, S. Bandow, K. Suenaga, H. Kato, T. Okazaki, H. Shinohara, and S. Iijima, Phys. Rev. B **64**, 115420 (2001).
[10] H. Kataura, Y. Maniwa, T. Kodama, K. Kikuchi, K. Hirahara, S. Iijima, S. Suzuki, W. Krätschmer, and Y. Achiba, in *Proceedings of the 25th International Conference on the Physics of Semiconductors*, edited by N. Miura and T. Ando (Springer, Heidelberg, 2001), p. 1609.
[11] H. Kataura, Y. Maniwa, M. Abe, A. Fujiwara, T. Kodama, K. Kikuchi, H. Imahori, Y. Misaki, S. Suzuki, and Y. Achiba, Appl. Phys. A: Mater. Sci. Process. **74**, 349 (2002).
[12] Y. Maniwa, H. Kataura, M. Abe, A. Fujiwara, R. Fujiwara, H. Kira, H. Tou, S. Suzuki, Y. Achiba, E. Nishibori, M. Takata, M. Sakata, and H. Suematsu, J. Phys. Soc. Jpn. **72**, 45 (2003).
[13] A. N. Khlobystov, R. Scipioni, D. Nguyen-Manh, D. A. Britz, D. G. Pettifor, G. A. D. Briggs, S. G. Lyapin, A. Ardavan, and R. J. Nicholas, Appl. Phys. Lett. **84**, 792 (2004).
[14] L. Guan, H. Li, Z. Shi, L. You, and Z. Gu, Solid State Commun. **133**, 333 (2005).
[15] M. Chorro, A. Delhey, L. Noé, M. Monthioux, and P. Launois, Phys. Rev. B (to be published).
[16] We note that, originally, lying and standing C_{70} molecular orientations were inferred from electron diffraction patterns (Refs. 9 and 10). Direct observations (electron microscopy images) were reported later (Refs. 13 and 14).
[17] K. H. Michel, B. Verberck, and A. V. Nikolaev, Phys. Rev. Lett. **95**, 185506 (2005).
[18] K. H. Michel, B. Verberck, and A. V. Nikolaev, Eur. Phys. J. B **48**, 113 (2005).
[19] B. Verberck and K. H. Michel, Phys. Rev. B **74**, 045421 (2006).
[20] C. J. Bradley and A. P. Cracknell, *The Mathematical Theory of Symmetry in Solids* (Clarendon, Oxford, 1972).
[21] A. V. Nikolaev, T. J. S. Dennis, K. Prassides, and A. K. Soper, Chem. Phys. Lett. **223**, 143 (1994).
[22] N. Hamada, S. I. Sawada, and A. Oshiyama, Phys. Rev. Lett. **68**, 1579 (1992); D. H. Robertson, D. W. Brenner, and J. W. Mintmire, Phys. Rev. B **45**, 12592 (1992).
[23] M. Sprik, A. Cheng, and M. L. Klein, Phys. Rev. Lett. **69**, 1660 (1992).
[24] M. Sprik, A. Cheng, and M. L. Klein, J. Phys. Chem. **96**, 2027 (1992).
[25] A. V. Nikolaev and K. H. Michel, Phys. Rev. B **54**, 12733 (1996).
[26] S. Reich, C. Thomsen, and J. Maultzsch, *Carbon Nanotubes* (Wiley-VCH, Weinheim, 2004).
[27] R. Sachidanandam and A. B. Harris, Phys. Rev. B **49**, 2878 (1994).
[28] C. Christides, T. John, S. Dennis, K. Prassides, R. L. Cappelletti, D. A. Neumann, and J. R. D. Copley, Phys. Rev. B **49**, 2897 (1994).
[29] A. K. Callebaut and K. H. Michel, Phys. Rev. B **52**, 15279 (1995).
[30] The coefficients $w_l^t(\lambda_t, R_T) = g_l^t(\lambda_t)\tilde{v}_l^t(R_T, \lambda_t)$, Eq. (A14), also contain molecular structure information via the molecular form factors $g_l^t(\lambda_t)$, Eq. (A11b). The pair potential characteristics enter via the integrals $\tilde{v}_l^t(R_T, \lambda_t)$, Eq. (A6).
[31] Gerardus Mercator (1512–1594), Flemish cartographer, invented the cylindrical projection. The angles β and γ play the role of geographical latitude and longitude, respectively.
[32] K. S. Troche, V. R. Coluci, S. F. Braga, D. D. Chinellato, F. Sato, S. B. Legoas, R. Rurali, and D. S. Galvao, Nano Lett. **5**, 349 (2005).
[33] S. Okada, M. Otani, and A. Oshiyama, New J. Phys. **5**, 122 (2003).
[34] P. M. Chaikin and T. C. Lubensky, *Principles of Condensed Matter Physics* (Cambridge University Press, Cambridge, 1995), Chap. 6.
[35] L. A. Girifalco, M. Hodak, and R. S. Lee, Phys. Rev. B **62**, 13104 (2000).
[36] The Lennard-Jones model of Chorro *et al.* (Ref. 15) gives a slightly too high equilibrium a value ($a = 10.1$ Å), though.
[37] The lowest value I_{33} of the C_{70} molecule's inertia tensor yields $\hbar^2/I_{33}k_B \approx 0.0065$ K.
[38] H. E. Stanley, *Phase Transitions and Critical Phenomena* (Clarendon, Oxford, 1971).
[39] H. Wagner, Phys. Rev. Lett. **25**, 31 (1970).
[40] V. J. Emery and J. D. Axe, Phys. Rev. Lett. **40**, 1507 (1978).
[41] F. Simon, Á. Kukovecz, C. Kramberger, R. Pfeiffer, F. Hasi, H. Kuzmany, and H. Kataura, Phys. Rev. B **71**, 165439 (2005).